RSC Advances

PAPER

View Article Online
View Journal | View Issue



Cite this: *RSC Adv.*, 2022, **12**, 21836

# Colorimetric and naked-eye detection of arsenic(III) using a paper-based microfluidic device decorated with silver nanoparticles†

Arezoo Saadati,[abc] Fatemeh Farshchi,[d] Mohammad Hasanzadeh, *[be] Yuqian Liu [a] and Farzad Seidi *[a]

Arsenic (As) as a metal ion has long-term toxicity and its presence in water poses a serious threat to the environment and human health. So, rapid and accurate recognition of traces of As is of particular importance in environmental and natural resources. In this study, a fast and sensitive colorimetric method was developed using silver nano prisms (Ag NPrs), cysteine-capped Ag NPrs, and methionine-capped Ag NPrs for accurate detection of arsenic-based on transforming the morphology of silver nanoparticles (AgNPs). The generated Ag atoms from the redox reaction of silver nitrate and As(III) were deposited on the surface of Ag NPrs and their morphology changed to a circle. The morphological changes resulted in a change in the color of the nanoparticles from blue to purple, which was detectable by the naked eye. The rate of change was proportional to the concentration of arsenic. The changes were also confirmed using UV-Vis absorption spectra and showed a linear relationship between the change in adsorption peak and the concentration of arsenic in the range of 0.0005 to 1 ppm with a lower limit of quantification (LLOQ) of 0.0005 ppm. The proposed probes were successfully used to determine the amount of As(III) in human urine samples. In addition, modified microfluidic substrates were fabricated with Ag NPrs, Cys-capped Ag NPrs, and methionine-capped Ag NPrs nanoparticles that are capable of arsenic detection in the long-time and can be used in the development of on-site As(III) detection kits. In addition, silver nanowires (AgNWs) were used as a probe to detect arsenic, but good results were not obtained in human urine specimens and paper microfluidic platforms. In this study, for the first time, AgNPs were developed for optical colorimetric detection of arsenic using paper-based microfluidics. Ag NPrs performed best in both optical and colorimetric techniques. Therefore, they can be a promising option for the development of sensitive, inexpensive, and portable tools in the environmental and biomedical diagnosis of As(III).

Received 4th May 2022
Accepted 11th July 2022

DOI: 10.1039/d2ra02820d

rsc.li/rsc-advances



## 1. Introduction

As a heavy metal, arsenic is the twentieth most plentiful element in the Earth's crust and the twelfth most plentiful element in the human body and is an ongoing pollutant owing to long-term toxicity. This substance is present in various forms with different oxidation states (0 in elemental arsenic, −3 in $AsH_3$, (IV) in arsenic acid, (III) in arsenous acid, and (II) in $As_4S_4$).[1] Arsenic in aqueous media is predominantly inorganic in the form of $As^{5+}$ (pentavalent arsenate) or $As^{3+}$ (oxyanions of trivalent arsenite).[2] $As^{3+}$ (as $H_3AsO_3$) is 60 times more toxic than $As^{5+}$ (as $H_3AsO_4$), and its presence in drinking water poses a serious threat to the environment and human health. According to the World Health Organization, the permissible level of arsenic in drinking water is less than 10 ppb, and excessive consumption leads to increased kidney, brain, and heart disease and increases the risk of skin, lung, and bladder cancer.[3,4]

Therefore, the detection of arsenic levels is of particular importance both in the environment and natural resources and in the human body. For this purpose, various analytical methods such as ICP-MS (inductively coupled plasma mass spectrometry),[5] atomic absorption/emission spectroscopy,[6] ion-selective electrode,[7] fluorescence spectrometry,[8] voltammetry,[9] X-ray fluorescence,[10] surface enhanced Raman scattering,[11] spectrophotometry,[12] and high-performance liquid

[a]Jiangsu Co-Innovation Center for Efficient Processing and Utilization of Forest Resources, International Innovation Center for Forest Chemicals and Materials, Nanjing Forestry University, Nanjing 210037, China. E-mail: f_seidi@njfu.edu.cn

[b]Pharmaceutical Analysis Research Center, Tabriz University of Medical Sciences, Tabriz, Iran. E-mail: hasanzadehm@tbzmed.ac.ir

[c]Central European Institute of Technology, Brno University of Technology, Brno CZ-612 00, Czech Republic

[d]Fundação Oswaldo Cruz, Instituto Oswaldo Cruz, Laboratório de Biologia Molecular e Doenças Endêmicas, Avenida Brasil No. 4365 – Manguinhos, Rio de Janeiro 21040-900, RJ, Brazil

[e]Nutrition Research Center, Tabriz University of Medical Sciences, Tabriz, Iran

† Electronic supplementary information (ESI) available. See https://doi.org/10.1039/d2ra02820d

chromatography[13] have been developed. However, these techniques require expensive instruments, pure chemicals, trained labor, various treatment processes, and laboratory environments. On the other hand, developing countries do not have the proper infrastructure to perform complex tasks. So, researchers are using simple methods like colorimetric and UV-Vis spectroscopy as an alternative method.[14] Although UV-Vis spectroscopy has potential advantages such as low cost and ease of use, they have limited use for on-site applications due to the need for electricity. Therefore, a cheap and easy method such as colorimetric detection in the solution phase can be a good alternative, which seems to be the most popular method among users due to time and cost savings.[15] To increase the sensitivity, speed, accuracy, efficiency, and cost-effectiveness of colorimetric sensors, various types of advanced nanoparticles (NPs) have been utilized in this matter.[16–23]

Nanostructures have attracted much attention in the field of metal ion analysis due to their unique optical traits. The basic principle of nanoparticle-based detection of metal ions is the accumulation of NPs because of interaction with heavy metal ions and their color change. The change in color intensity of the nanoparticle solution is proportional to the analyte concentration, which is monitored using UV-Vis spectroscopy.[24,25] Metal NPs such as silver and gold have attracted a lot of attention in this field due to their high extinction coefficient and unique optical properties. These properties are known as surface plasmon resonance (SPR) and are attributed to mass bipolar oscillation, making silver nanoparticles (AgNPs) desirable for colorimetric-based detection of heavy metal ions.[26] Because the position and intensity of the absorption band in the visible spectrum change because of the interaction between the analyte and the NPs, this process can be seen even with the naked eye. The optical properties of NPs are proportional to their size and structure.[27] Silver triangular NPs have strong SPR properties and can be adjusted across the visible area by adjusting the length and thickness of the edges and the tip morphology of the nanoplate. These structures have special optical, chemical, and electronic properties compared to spherical AgNPs due to their three sharp heads.[28] However, colorimetric-based sensors in the solution phase have limitations such as the need for trained personnel and complex steps. To develop cheaper, more reliable, and disposable methods with on-site diagnostics without the need for electrical connections, researchers began modifying existing methods or exploring new diagnostic strategies.

The microfluidic systems were proposed by scientists as a suitable solution for the development of simple and inexpensive tools.[29–31] Paper-based microfluidics are made by creating hydrophilic channels using hydrophobic barriers and are as portable as traditional microfluidic devices.[32] In addition, they can perform multiple measurements and process small volumes of fluids. Traditional microfluidics is made of glass, silicon, and polymers (such as PDMS (polydimethylsiloxane) and poly(methyl methacrylate) (PMMA)) and requires a cleanroom to build. Interestingly paper-based microfluidics is made from affordable materials and does not require a cleanroom or computer-controlled pumps to operate. These features make paper microfluidics the ideal medium for developing point-of-care diagnostic tests in all areas.[33,34] In this study, a novel diagnostic platform was presented for the rapid and accurate recognition of As(III) using UV-Vis spectroscopy technique and colorimetric assay. AgNPs containing Ag NPrs, Cys-capped Ag NPrs, Met-capped Ag NPrs, and AgNWs were first used as diagnostic probes. The change in color and absorption spectrum as a result of the interaction between the sensing probes and the arsenic ions indicates the ability of the developed method to sensitive recognition of arsenic in real samples. Therefore, the ability of probes to detect arsenic in human urine samples was evaluated, and except for AgNWs, other probes performed well. In addition, the ability of the designed microfluidics in the arsenic on-site analysis was also evaluated. This simple and inexpensive strategy has shown potential for the development of arsenic diagnostic kits.

## 2. Experimental

### 2.1. Instruments

U-3010 spectrophotometer (Hitachi, Japan) was employed for UVVis spectroscopy analysis. The particle size and morphology of NPs were assessed by transmission electron microscope (TEM) (Adelaide, Australia-with an operating voltage of 200 kV). The dynamic size of NPs was investigated using an atomic force microscope (AFM) with Nanosurf (AG Gräubernstrasse 12, 4410 Liestal Switzerland) in a tapping mode. High-resolution field-emission scanning electron microscopy (FE-SEM, Hitachi-Su8020, Czech-with a working voltage of 3 kV) was applied for assessment of synthesized NPs surface morphology. Energy-dispersive spectroscopy (EDS) was carried out for the appraisal of the elemental composition of NPs. Surface charge and size distribution were also evaluated by zeta potential measurement, Zetasizer Ver. 7.11 and dynamic light scattering (DLS) analysis (Malvern Instruments Ltd, MAL1032660, England).

### 2.2. Materials and reagents

The solution of ions (As(III), Ti(II), Fe(III), W(IV), Pt(II), V(III), Zr(IV), Hg(II), Mg(II), Se(IV), Ba(II), Sr(II), Te(II), Mo(II), K(I), Cr(II), Bi(III), Zn(II), Li(II), Mn(II), B(III), Na(I), Ca(II), Al(III), Si(II), Co(II), Cs(II), Ni(II)) with 1 ppm concentration were acquired from Chemlab Company (Zedelgem, Belgium). Tri-sodium citrate (TSC) ($Na_3C_6H_5O_7$) (99.0%), L-cysteine (97%), methionine (99%), methanol (≥99.8%), PVP K-30 (polyvinyl pyrrolidone), sodium borohydride ($NaBH_4$), silver nitrate ($AgNO_3$), hydrogen peroxide ($H_2O_2$, 30 wt%) and ethylene glycol (EG) were attained from Sigma-Aldrich (Ontario, Canada).

### 2.3. Synthesis of optical probes

**2.3.1. Silver nanowire.** Ag NWs were synthesized by our previous work.[35] Concisely, EG (20 mL) containing PVP (0.668 g) was stirred at 170 °C for 20 to 30 min. Then, AgCl (0.05 g) was added to this mixture. After 3 min stirring, $AgNO_3$ (0.22 g plus 10 mL EG) was added to it and stirred at the same temperature for 30 min. Eventually, to remove non-reacted EG, PVP, and

other impurities, centrifugation by methanol was performed at 6000 rpm for 30 min.

**2.3.2. Silver nanoprism.** The synthesis of Ag NPrs (silver nanoprism) was performed according to our prior work.[36] Briefly, 0.01 M of Ag $NO_3$ solution was added to the 203 mL water comprising PVP. After stirring, 0.075 M TCS solution and $H_2O_2$ were added to this solution, respectively. Conclusively, $NaBH_4$ (100 mM) as a reducing agent was added which led to discoloration. After 30 min stirring, the blue colloidal mixture was obtained and was kept at 4 °C.

### 2.4. Optical determination of As(III)

Optical identification of arsenic(III) by using Ag NPs as a sensing probe was carried out at room temperature in the wavelength range of 200–800 nm. To do so, As(III) with an equal volume ratio was added to the sensing probe and the UV-Vis were recorded in a quartz cuvette.

### 2.5. Colorimetric detection of As(III)

For the colorimetric recognition of As(III), the color change was monitored by a mobile phone camera under a natural light source in a solution and paper-based analytical device.

### 2.6. μPCD manufacture

The paper-based microfluidic chip pattern was created by CorelDRAW software. The chips have substrate storage that is connected through eight channels with eight detection zones (Scheme S1 (see ESI†)). These chips were produced using the technique developed in our previous report.[37]

## 3. Results and discussion

### 3.1. Selection of Ag nanoparticle as a sensing probe for detection of As(III)

The interaction of NPs with heavy metal ions leads to the accumulation of NPs and their color change, which can be considered as the basic principle of colorimetric identification of metal ions using NPs.[24,38] A variety of NPs have been used in colorimetric studies, among which metal NPs of Au and Ag have attracted the attention of researchers.[24,39] These NPs have been widely used in the efficient analysis of toxic heavy metals due to their unique optical properties and high extinction coefficient.[40] These properties are known as SP (surface plasmon) which is attributed to combined bipolar oscillation.[41] This phenomenon has made AgNPs a very desirable and practical option for detecting different types of heavy metals due to interaction with the analyte and changes in the position and intensity of absorption of the visible spectrum. Even this process can be seen with the naked eye.[42] Therefore, in this work, AgNPrs and AgNWs were used as sensing probes for the accurate monitoring of As(III).

Because smaller colloidal particles can absorb visible light through SPR motion, capping or stabilizing agents can be used to prevent NPs from binding or accumulating with other particle components.[43,44] Hence, cysteine (Cys) and methionine (Met) were used as additives. The additives are attached to the Ag NPrs surface *via* an Ag–S bond by thiol terminals and modify the sensing probes. The enclosure of NPs with additives leads to electrostatic repulsion between them. Silver atoms are strongly bonded to electron-rich sites due to their performance among the highest.[38,45] These cumulative negative charges carried through the nanoparticle domain are separate and increase the stability of the NPs. Cysteine acts as an adsorbent due to its thiol, amine, and carboxylate sites.[46] Arsenic has a positive charge and can strongly interact with the negative charge of oxygen (O–H) in the additive-sensing probe system and lead to aggregation which is necessary for the colorimetric recognition of the target.[47,48]

### 3.2. Characterization of sensing probes

**3.2.1. Ag NPrs.** Characterization of the proposed sensing probes was investigated using UV-Vis spectroscopy, DLS, zeta potential, SEM, TEM, and AFM techniques. UV-Vis is one of the easiest methods to identify metal NPs that are widely used in discovering their shape and size. As shown in Fig. S1 (see ESI†), the prepared Ag NPrs are blue and have UV-Vis absorption at wavelengths 337, 477, and 705 nm. The first two absorption bands (337 and 477 nm) correspond to out-of-plane and in-plane quadrupole resonance of Ag NPrs, respectively. The 705 nm band can also be attributed to the Ag NPrs in-plane dipole resonance.[49,50] Zeta potential measurement is a feasible technique for investigating the surface charge of NPs and their stability. NPs with zeta potential greater than +30 and −30 mV have high stability and with increasing zeta potential, particle size increases and aggregation decreases.[51] The zeta potential of the prepared NPs was −67.5 mV, which indicates their proper stability (Fig. S2 (see ESI†)). Particle distribution profiles were evaluated using DLS. The synthesized NPs have a radius of 0.84 nm as shown in Fig. S3A.† DLS in the presence of arsenic was also examined to investigate the interaction of the analyte with the probe and its aggregation of them. An increase in the number of particles with a high hydrodynamic radius (99.27 nm) indicates the accumulation of NPs in the presence of an analyte (Fig. S3B (see ESI†)). Also, the surface morphology and sample composition were analyzed using FE-SEM. The recorded images exhibit the triangular structure (Fig. S4 (see ESI†)). The recorded EDS spectrum also confirms the presence of Ag elements (Fig. S5 (see ESI†)). HR-TEM imaging was performed for direct imaging of atomic structures and crystallographic specimens. As displayed in Fig. S6 (see ESI†), the synthesized NPs have a triangular structure. Also, the three-dimensional surface structure and topology of synthesized NPs were evaluated using AFM. Ag triangular NPs with white corners are visible on the surface (Fig. S7 (see ESI†)). Therefore, Ag NPrs were synthesized successfully.

**3.2.2. Cys-capped Ag NPrs.** The discoloration of Ag NPrs in the presence of analytes as a result of their aggregation provides a proper colorimetric system for the detection of As(III). Thiol-containing organic compounds can be applied to alter nanoparticle superficies and organize self-assembly.[52–54] L-Cysteine is a non-essential amino acid whose functional groups can act as a hydrophilic interface in the interaction between the analyte

and the Ag NPrs surface.[55] The thiol group helps binding of Cys to the surface of Ag NPrs. Amino (–$NH_2$) and carboxylic (–COOH) groups also lead to the stabilization of NPs.[56] Therefore, we adopted the amino acids Cys as additives to modify the surface of Ag NPrs. As shown in Fig. S8 (see ESI†), UV-Vis absorption at peak wavelengths 337, 477, and 705 nm is greatly reduced compared to Ag NPrs. There was no change in the absorption position. Also, no significant color change was observed and only the Cys-capped Ag NPrs were slightly lighter. The surface charge of the particles in Cys-capped Ag NPrs is −20 mV (Fig. S9 (see ESI†)). The particle size of Cys-capped Ag NPrs is about 146.3 nm, which increases to 317 nm with the addition of arsenic ion (Fig. S10A and B (see ESI†)).

**3.2.3. Met-capped Ag NPrs.** In this work, methionine (Met) was also evaluated as an additive in sensing probes due to the presence of thiol, amino and carboxylic functional groups. As shown in Fig. S11 (see ESI†), the absorption peak intensity corresponding to a wavelength of 337 nm has decreased compared to Ag NPrs, and the color of the solution was changed to light blue, which confirmed the successful formation of Met-capped AgNPrs. The peak related to wavelengths 477 and 705 nm has a significant decrease in absorption and the peak related to wavelength 705 nm has shifted to a lower wavelength. The surface charge of Ag NPrs is −21.5 mV (Fig. S12 (see ESI†)). The particle distribution study, the results of which are presented in Fig. S13 (see ESI†), revealed that the particle size increases from 14.52 nm to 433.8 nm after the addition of arsenic(III) with this optical probe (Met-capped Ag NPrs).

**3.2.4. Ag NWs.** The optical attributes of the synthesized Ag NWs were appraised using UV-Vis spectroscopy. Ag NWs have an anisotropic form and induce two plasmon bands including a longitudinal plasmon band and a transverse plasmon band (corresponding to the electronic change along the rod's short axis). This trait distinguishes them for use in a wide range of spectroscopic studies.[57,58] The formation of Ag NWs is endorsed by the appearance of absorption bands at 298 and 420 nm (Fig. S14 (see ESI†)). Zeta-potential examinations demonstrated that NPs have a surface charge of −2.05 mV (Fig. S15†). The hydrodynamic diameter of the NPs was assessed in the presence of the analyte. According to Fig. S16 (see ESI†), as the analyte increases, the diameter increases from 465.8 nm to 1826 nm, indicating the interaction of Ag NWs and the analyte. Surface imaging was performed using FE-SEM to evaluate the morphology of Ag NWs. The recorded images are presented in Fig. S17 (see ESI†). The presence of silver in the nanoparticle structure was revealed by EDS (Fig. S18 (see ESI†)). Three-dimensional surface topology was also performed using AFM imaging. As can be seen in Fig. S19 (see ESI†), the synthesis of the desired structures has been done successfully.

*Optimization of additive-probe ratio.* As previously mentioned, arsenic as a semi-metal and toxic element is very dangerous to human health and can lead to a variety of diseases, including cancer.[59] Therefore, the development of simple and inexpensive systems to monitor it is very valuable. So, several sensing probes were evaluated for rapid and accurate identification of As(III) in real samples. Due to the more favorable results obtained from Ag NPrs, various additives were used to cap them. The nature and number of additives affect the optical properties of NPs. Hence, different volume ratios of the amino acids cysteine and methionine (as additives) were mixed with Ag NPrs (1 to 6, including Ag NPrs, 1 : 1, 1 : 2, 2 : 1, 1 : 3 and 3 : 1 ratio of Ag NPrs and additive, respectively). After 10 minutes of storage at room temperature, color changes were visually examined. The results are presented in Fig. S20 (see ESI†), which reveals that the best case is related to the 1 : 3 ratios of additive and Ag NPrs. When a 1 : 3 ratio additives is combined with a probe, there is no significant change in the color of the probe, whereas, in the presence of the analyte, the color changes obtained from the capped probe are different from the non-capped probe. Then, arsenic (1 ppm) was added to the sensing probes in a 1 : 1 ratio, and the color change was evaluated in the presence of it. Under experimental conditions, the cysteine and methionine molecules attached to the surface of Ag NPrs are negatively charged. Electrostatic interactions between the positive charge of arsenic and the surface of modified sensing probes can lead to the accumulation of AgNPs in a mixture solution.

### 3.3. Optical detection of As(III) in solution

Optical examinations were performed using UV-Vis spectroscopic technique in solutions prepared from sensing probes based on AgNPs. First, the capability of the introduced probes in the detection of arsenic was evaluated. Then, the sensitivity and selectivity of the sensing probes in the standard and real samples were investigated.

**3.3.1. Investigation of detection behavior of sensing probes.** Nanomaterials, like metal NPs, are identified by their various physical and chemical traits.[60] These features are proportional to the surface to volume ratio. The surface-to-volume ratio increments as the particle size decreases and the surface area increases.[61,62] Hence, surface atoms and molecules play an essential role in NPs and affect the traits of NPs. Among the physical and chemical qualities, optical properties are of exceptional importance and are often employed in quick and easy measurement methods.[63] The interaction of light with nanosystems leads to some events such as transmission, absorption, reflection, light scattering, transmission, and fluorescence.[58] For example, Ag NPs are detected by specific absorption bands of a certain intensity, but the bond properties change as a result of changes in the external environment or exposure to analytes.[64] This sensitivity to the external environment can be used in the field of optical chemosensing of specific analytes. When the light beam strikes the solution, a surface plasmon phenomenon occurs, which indicates the presence of NPs and is seen as a sharp peak in the visible region.[65] Local surface plasmon resonance (SPR) is a specific phenomenon in metal NPs, especially AgNPs, and depends on the dielectric constant of its surroundings.[62]

Due to their free electrons, Ag NPs produce a light effect known as the surface plasmon absorption band, which results from the combined vibration of the electron NPs in the light wave resonance at the aqueous suspension.[58] Increasing the size of the NPs causes the plasmon absorption to move towards a lower energy wavelength and the color red. In addition, the

peak of absorption becomes wider, which indicates the growth of the suspension and the formation of aggregation. The presence of an analyte leads to a constant dielectric change that appears as a change in color and a change in the location and intensity of absorption.[66] So, UV-Vis spectroscopy of the sensing probes (AgNPrs, Cys-capped AgNPrs, Met-capped AgNPrs, and AgNWs) was recorded before and after interaction with the candidate analyte (with a volume ratio of 1 : 1). In the UV-Vis absorption spectra recorded in the presence of arsenic (Fig. 1), an absorption peak of 305 nm is observed, which confirms the accumulation in the NP's presence of the analyte.

In other words, the plasmon traits of the NPs are altered in the presence of analytes. As can be seen in colorimetric studies, Ag NPrs are blue with a negative surface charge (Scheme 1). As a result of the addition of positively charged arsenic, $AgNO_3$ is reduced to Ag atoms deposited on the Ag NPrs surface, resulting in deformation from Ag NPrs to Ag NPs.[67] As can be seen, the prepared Ag NPrs are blue and have UV-Vis absorption at wavelengths of 337, 477, and 705 nm. The first two absorption bands (337 and 477 nm) correspond to out-of-plane and in-plane quadrupole resonance of Ag NPrs, respectively.[49,50] The 705 nm band can also be attributed to the Ag NPrs in-plane dipole resonance. The peak of in-plane bipolar resonance is strongly dependent on the Ag NPrs shape. This phenomenon, which is used in the design of sensors based on wavelength changes, can be attributed to changes in the morphology of Ag NPrs and the tendency of newly produced Ag atoms to deposit at the Ag NPrs surface.[68]

The resulting deformation is also seen visually in the color of the solution, allowing arsenic analysis in both the solution and leading to a change of UV-Vis spectrum wavelengths. As time goes on and the redox reaction between arsenic and silver ions is completed, the newly produced silver atoms on the Ag NPrs produce circular nanoplates that change the color of the solution to orange.[28] Despite discoloration of the detection probe solutions after one hour in the presence of the analyte, no significant changes in the absorption peak intensity were observed at the 300 nm wavelength. In fact, at the beginning of the Ag NPrs interaction with As(III), $AgNO_3$ is reduced to Ag atoms deposited on the surface of Ag NPrs, converting the Ag NPrs to Ag NPs. Morphological changes lead to a change in the color of NPs from blue to purple, which can be detected by the naked eye. Over time, the redox reaction between the arsenic and silver ions was completed, and the newly formed silver atoms on the Ag NPrs formed circular nanoplates, changing the color of the orange solution.

Under experimental conditions, the cysteine and methionine molecules attached to the surface of Ag NPrs are negatively charged. Electrostatic interactions between the positive charge of arsenic and the surface of modified detection probes can lead to the accumulation of Ag NPs in solution. After one hour, no change in the color of the methionine-modified sensing probe was observed, while the peak intensity of adsorption decreased. In the cysteine-modified probe, a slight discoloration was observed in the solution after one hour, but no significant changes were observed in the peak intensity of adsorption.

Ag NWs have an anisotropic form and induce two plasmon bands including a longitudinal plasmon band and a transverse plasmon band (corresponding to the electronic change along the short axis of the rod).[58] This feature distinguishes them for use in a wide range of spectroscopic studies. As can be seen, no significant discoloration is seen in Ag NWs probes in the presence of analytes, while spectroscopic examination shows the ability of this probe to detect arsenic. Over time, no change in spectroscopic and colorimetric results was observed and only sediment was observed. These results indicate that the proposed sensing probes are capable of arsenic(III) detection by new mechanisms.

**3.3.2. Analytical evaluation for determination of As(III).** According to the results of the examination of the ability of introduced sensing probes to the monitoring of arsenic(III), their ability at low concentrations of analyte was also evaluated. Therefore, the relationship between As(III) concentration and adsorption was determined by UV-Vis spectrophotometric measurements of separate reaction systems. For this purpose, As(III) solutions with different concentrations (0.0005, 0.001, 0.005, 0.01, 0.05, 0.1, 0.2, 0.3, 0.4, 0.6, 0.7, 0.8 and 1 ppm) were prepared and mixed with sensing probes (AgNPrs, Cys-capped Ag NPrs, Met-capped AgNPrs and AgNWs) in a volume ratio of 1 : 1. The absorption spectra recorded in the range of 250 to 800 nm are exhibited in Fig. 2. In addition, the adsorption *versus* concentration ratio is also presented in Fig. 2. Then, important analytical parameters such as linear range and lower limit of quantification (LLOQ) were obtained from calibration curves plotted through absorption changes in the 304 nm band at different concentrations of As(III). As can be seen, there is a significant linear relationship between the absorbance of probes in the concentration range of 0.0005 to 1 ppm of As(III). At high concentrations of arsenic, in addition to adsorption in the 305 nm band, a displacement at the peak of in-plane dipolar resonance (705 nm) is also observed in the LSPR spectrum, which is accompanied by a change in solution color from blue to yellow. This phenomenon can be attributed to changes in the morphology of Ag NPrs and the tendency of silver atoms to deposit on their surface.[28] It should be noted that the amount of adsorption in this band is not related to the concentration of the analyte. At low concentrations of arsenic, the adsorption decreases in the 304 nm band and increases in the 715 nm band, which can be attributed to the fact that the morphology of sensing probes (Ag NPrs, Cys-capped Ag NPrs, Met-capped AgNPrs) did not change at low concentrations of the analyte. A comparison of developed Ag NPs-based colorimetric biosensors for the detection of As(III) is presented in Table 1.

As can be seen, there is no report on the detection of As(III) based on the sensing probes introduced in this study, which is one of the benefits of this work. The ability of proposed probes for arsenic examination was evaluated using UV-Vis spectroscopic technique. A comparison of the analytical performance of the presented sensor with previous studies shows that this sensor is more sensitive to them and can detect As(III) in a wider linear range. In addition, colorimetric studies were performed using paper-based microfluidics, which indicates the potential performance of these microfluidics in the development of As(III) diagnostic kits.

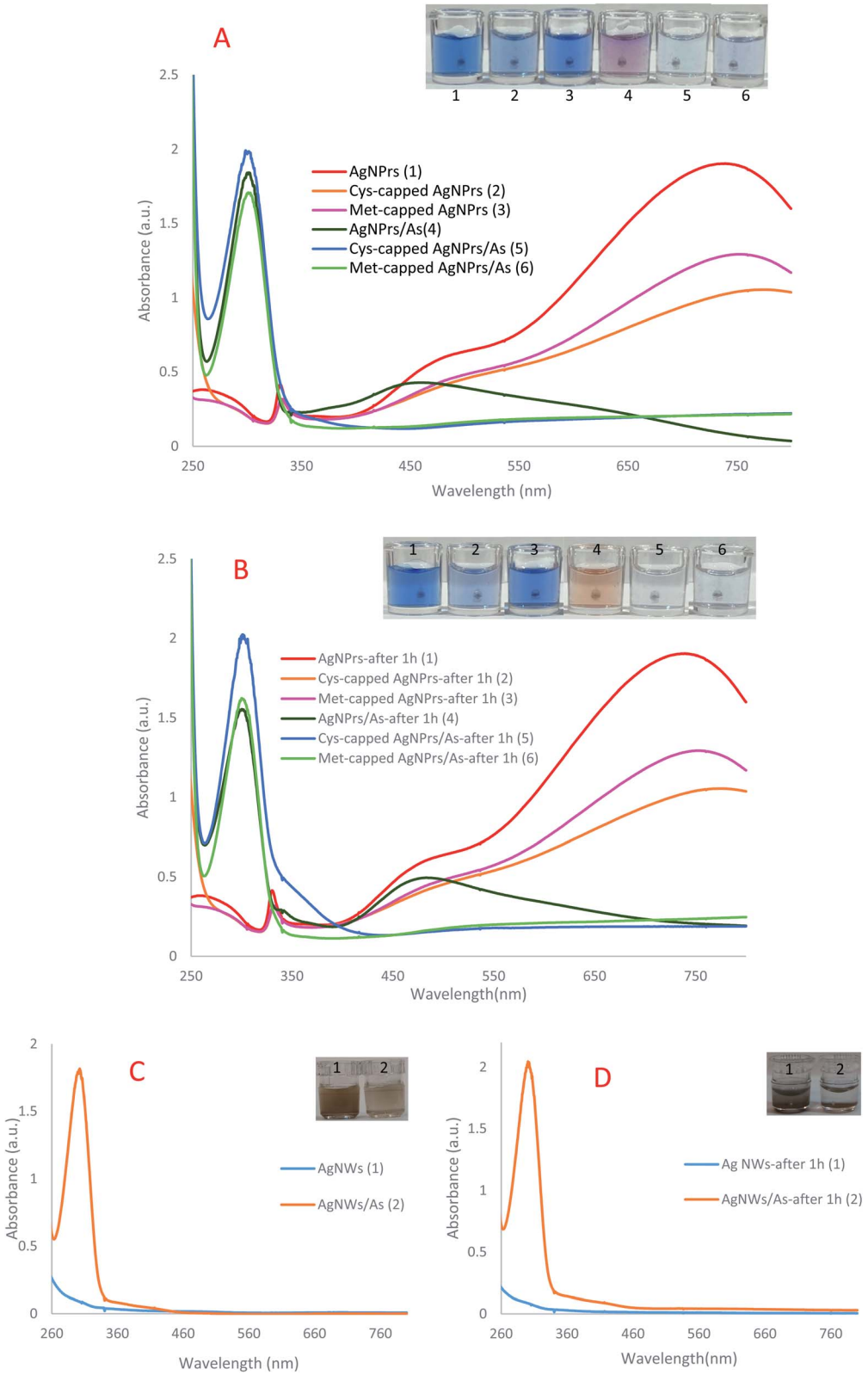


Fig. 1 The UV-Vis spectra of sensing probes in the presence and absence of arsenic (A) AgNPrs, Cys-capped AgNPrs, Met-capped AgNPrs; (B) AgNPrs, Cys-capped AgNPrs, Met-capped AgNPrs after 1 h; (C) AgNWs and (D) AgNWs after 1 h.

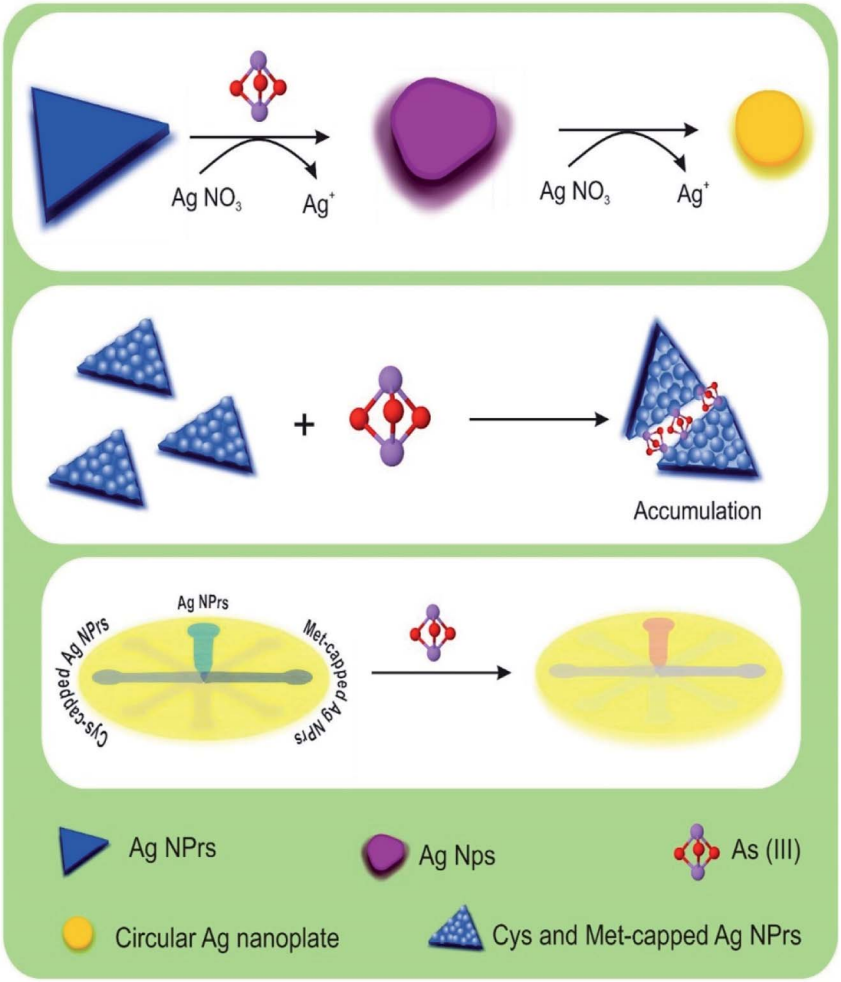


Scheme 1 Schematic illustration of naked-eye detection of As(III) by colorimetric assay based on AgNPs.

**3.3.3. Analytical evaluation for As(III) determination in real sample.** Arsenic poisoning has been reported in various parts of the world.[73] These poisonings affect all organs of the body and every year, many victims of severe poisoning suffer from severe symptoms or even death. Arsenic compounds are present in the environment and the human body in inorganic and organic forms.[74] Arsenic, especially inorganic arsenic, is well absorbed through the gastrointestinal tract (80–90%) and will be distributed throughout the body. It is often metabolized by methylation and is excreted mainly in the urine.[75] Methylation of inorganic arsenic compounds is said to undergo a detoxification process.[76] Arsenic compounds lead to lipid peroxidation damage and reduced antioxidant defense levels. Contamination of various sources with arsenic compounds, especially inorganic arsenic, has caused great concern for human health.[77] Prolonged exposure to arsenic can cause cancers of the skin and internal organs, including liver, lung, kidney, and bladder, as well as increase mortality. The noncancerous effects of oral arsenic include clinical manifestations in the gastrointestinal, cardiovascular, pulmonary, immunological, neurological, endocrine (such as diabetes), and skin systems. Tests to diagnose poisoning are based on the blood concentration of arsenic, its concentration in urine, hair, and nails.[78–80] Measurement of urinary arsenic concentration is the most valid test for people who have been exposed to it.[75] Therefore, in this study, arsenic concentrations were evaluated by the spike method in human urine specimens. For this purpose, various concentrations of arsenic (0.0005, 0.001, 0.005, 0.01, 0.05, 0.1, 0.2, 0.3, 0.4, 0.6, 0.7, 0.8 and 1 ppm) were prepared and mixed with human urine samples in a volume ratio of 1 : 1. Then, the prepared mixtures were mixed with a 1 : 1 ratio with candidate probes, and their interaction was evaluated using UV-Vis spectroscopic technique. Colorimetric analysis was also performed using a mobile camera. The recorded absorption spectra and the calibration curves resulting from the adsorption changes at different concentrations are obtained (Fig. S21 (see ESI†)). The results revealed that the AgNWs probe was not able to detect As(III) in the urine sample. Analytical parameters obtained from other probes are presented in Table S1 (see ESI†). As it turns out, the Cys-capped Ag NPrs probe detects a wide linear range of As(III), and compared to the other two probes (AgNPrs and Met-capped AgNPrs) it has a lower detection limit. Therefore, it can be said that for detection of As(III) in human urine samples, the Cys-capped Ag NPrs probe exhibits better performance.

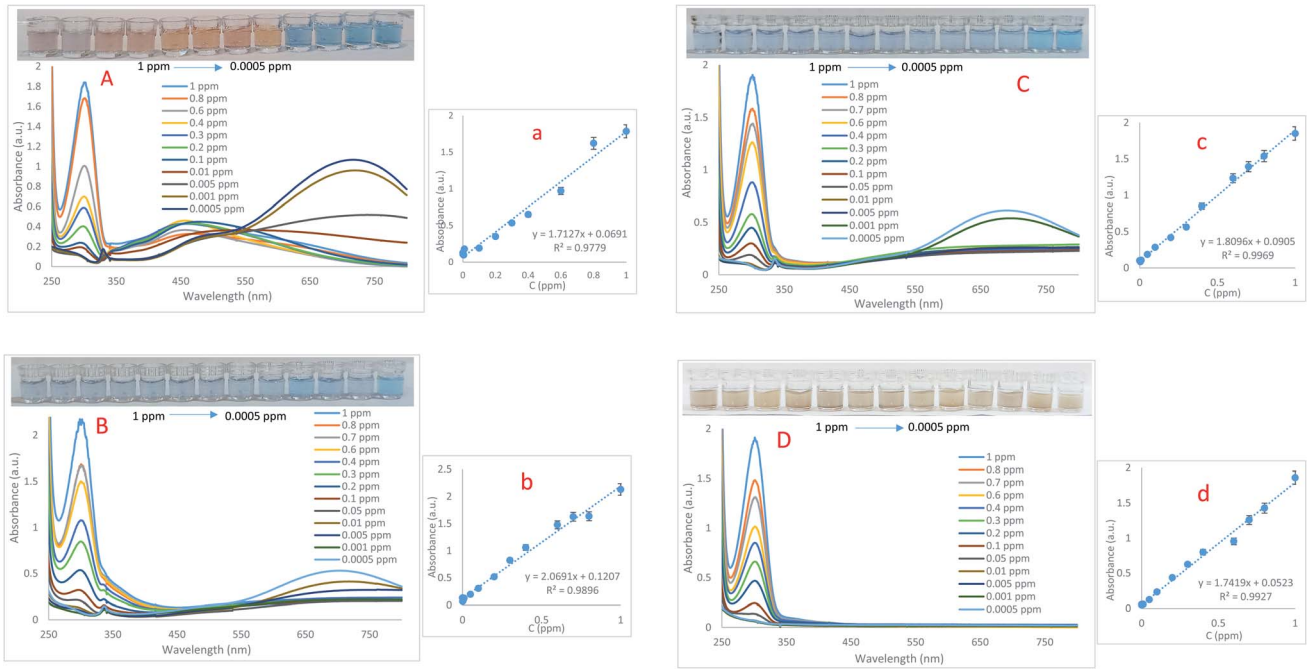


Fig. 2 The UV-Vis spectra of (A) AgNPrs, (B) Cys-capped AgNPrs, (C) Met-capped AgNPrs and (D) AgNWs sensing probes and calibration curves in the presence of various concentration of arsenic (0.0005, 0.001, 0.005, 0.01, 0.05, 0.1, 0.2, 0.3, 0.4, 0.6, 0.7, 0.8 and 1 ppm).

**3.3.4. Selectivity of the analytical process in standard samples.** Selectivity is one of the most significant factors for the analytical evaluation of chemosensors.[81] Specificity indicates the ability of a sensing probe to detect an analyte in a specimen containing other contaminants.[82] Therefore, to evaluate the selectivity of the proposed probes for the recognition of As(III), their colorimetric and spectrophotometric behavior was done. For this purpose, various metal ions such as tin, iron, tungsten, platinum, vanadium, zirconium, mercury, magnesium, selenium, barium, strontium, tellurium, molybdenum, potassium, chromium, bismuth, zinc, lithium, manganese, boron, sodium, calcium, aluminum, silicone, cobalt, cesium, and nickel (1 ppm) were mixed with a volume ratio equal to the probes (Ag NPrs, Cys-capped Ag NPrs, Met-capped Ag NPrs, and Ag NWs). The results of colorimetric and optical examinations are presented in Fig. S22 (see ESI†). As can be seen, the probes not only change color in the presence of As(III) but also in the presence of other ions. Therefore, it can be said that probes can detect other ions in addition to As(III). It should be noted, however, that by observing the naked eye, the Ag NPrs and Ag NWs probes strongly have significant selectivity for the target analyte. Because the color change created in the presence of As(III) is different from other ions. While the location and amount of UV-Vis absorption in the presence of most ions is similar to arsenic. Cys and Met-capped Ag NPrs probes do not have good selectivity for the detection of arsenic ions. It should be noted that the introduced probes are not able to detect some metal ions such as tungsten, platinum, vanadium, zirconium, mercury, magnesium, selenium, and barium, silicone. In addition, the selective detection of arsenic in the presence of other ions under the same experimental conditions was evaluated (Fig. S23 (see ESI†)). For this purpose, each of the interveners was mixed with a volume ratio equal to the target analyte, then the resulting mixture was added to the sensing probe solution (1 : 1 v/v). Colorimetric and optical examinations were performed. The results indicated that the probes utilized could detect the target analyte in the presence of other metal ions and most metal ions did not interfere with the detection of the target analyte. However, some ions interfere with the detection of arsenic by increasing the amount of adsorption (such as Mg(II), Cr(III), K(I), Mn(II), *etc.*) or decreasing it (such as Ti(II), Si(II), Cs(II), *etc.*). In both cases of interfering investigation (separately and in

Table 1 Comparison of developed colorimetric biosensors based on AgNPs for the detection of As(III) with the present research

| Sensing probe | LOD/LLOD (ppm) | Linear range (ppm) | Ref. |
|---|---|---|---|
| GSH/DTT/Asn–AgNPs | 0.00036 | 0.0004–0.02 | 69 |
| AgNPls–$SiO_2$–Fh | 0.5 | 0.5–30 | 70 |
| AgNPls–$SiO_2$–Fh | 0.5 | 0.5–3 | 70 |
| Aptamer–AgNPs | 0.006 | 0.05–0.7 | 71 |
| PEG–AgNPs | 0.001 | 0.005–0.013 | 72 |
| AgNPrs, Cys-capped AgNPrs, Met-capped AgNPrs, AgNWs | 0.0005 | 0.0005–1 | Present work |

combination with the analyte) in the presence of some ions, a shift at the peak of the absorption band is observed. Changes in the absorption band in different optical probes are different. For example, in Ag NPrs optical probes, the adsorption band is shifted in the presence of Ti(II), Fe(III), W(IV), Pt(II), V(III), Zr(IV), Hg(II), Mg(II), Se(IV), Mo(II), Cr(III), Bi(III), Zn(II) and Cs(II), as well as in the combination of As(III) with Fe(III), W(IV), Pt(II), V(III), Zr(IV), Hg(II), Mg(II), Mo(II), Bi(III) and Zn(II). Absorbance band shift was observed in the presence of Ti(II), Fe(III), Pt(II), V(III), Zr(IV), Hg(II), Se(IV), Te(II), Mo(II), Bi(III), Si(II) and Cs(II) and the combination of As(III) with Fe(III), W(IV), Pt(II), V(III), Zr(IV), Mg(II), Ba(II), Sr(II), Mo(II), K(I), Bi(III), Zn(II), Li(II) and Al(III) using a Cys-capped Ag NPrs probe. Also in the Met-capped Ag NPrs probe, the absorption band shift was observed in the presence of Ti(II), Fe(III), W(IV), Pt(II), V(III), Zr(IV), Hg(II), Mo(II), Bi(III) and Cs(II) ions and the combination of As(III) with Fe(III), W(IV), Pt(II), V(III), Hg(II), Mo(II) and Bi(III). As shown in Fig. S22 and S23 (see ESI†), a shift in the absorption band is observed in the LSPR spectrum and is accompanied by discoloration of the solution. This phenomenon can be attributed to changes in the morphology of NPs and the tendency of silver atoms to deposit on their surface.[28]

**3.3.5. Stability of sensing probes.** NPs are out of equilibrium owing to their high surface energy and are unstable. Hence they easily change themselves or react with active ingredients.[83] The stability of NPs is often described in terms of their capability to remain the same in shape, size, and chemical composition.[84] Various particle sizes and shapes lead to different colors. The color of NPs is due to the intensification of SPR, which results from the resonance of the outer electron bands of the particles with the wavelength of light.[85] Therefore, changing the size and shape of the particles can affect the color of Ag NPs, and according to their color, the size of the particles can be understood.[86] Since the stability of NPs is a challenging issue in their application, in this study the stability of Ag NPrs-based sensing probes was evaluated. The blue solution is in the form of a small prism. As a result of the redox reaction in the presence of arsenic ions, the NPs form a nanoplate, and the particle size increases as a result of aggregation (Fig. S24A and a (see ESI†)). In addition to color change, the UV-Vis spectroscopic technique was exploited to examine the changes. The results exhibited that the nano prism itself is stable and after 20 days did not show any change in color and UV-Vis absorption. In the presence of arsenic ion, no change in color and UV-Vis absorption was observed over time. According to the obtained results, it can be concluded that Ag NPrs have long-term stability. In addition, the stability of NPs can be related to colloidal stability, which is true when NPs have a capping element. Capping agents on the surface of NPs prevent them from accumulating in the solution in which the nanoparticle is to be dispersed. Therefore, in this study, the stability of Ag NPrs capped with methionine and cysteine alone and in the presence of an analyte was evaluated. The results revealed that the Cys-capped Ag NPrs probe became completely colorless after 1 day (Fig. S24B and b (see ESI†)). Due to the increase in particle size in cysteine, it can be said that the capping agent did not protect the NPs well. Therefore, the particle size increases as the aggregation increases, and more particle growth over time leads to the loss of the chemically active surface of the particles. Met-capped Ag NPrs probe is stable on the first day of preparation and no color change is observed. But, from the second day, it starts to change color to purple. It can be said that the stability of this probe on the first day is desirable and as the accumulation of time increases and the particle size begins to enlarge and the color shifts to red. UV-Vis examinations also show that after one day, the amount of UV-Vis absorption by this probe begins to decrease. Therefore, it can be concluded that the most stable form of this detection probe is on the first day of its preparation (Fig. S24C and c (see ESI†)).

### 3.4. μPAD development for colorimetric detection of As(III)

Fast, selective, proprietary, and inexpensive tools are especially meaningful for on-site environmental surveys.[87] For the development of such devices, papers have been considered an appropriate substrate due to their advantages such as low cost, commercial availability, and easy design. In addition, papers are made of cellulosic fibers and are environmentally friendly, and due to their capillary properties, they can flow fluids into their channels without the need for a pump or external force.[88] Efforts to develop paper-based microfluidics for the detection of heavy metal ions have attracted tremendous research attention due to the increasing environmental pollution of metals and their adverse effects on human health. These tools have all the features of the WHO-approved diagnostic devices such as sensitivity, cost-effectiveness, user-friendliness, and portability.[89] Hence, μPADs have recently been used for the on-site monitoring of environment sites. Due to its excellent variability and hydrophilicity, the paper can facilitate the adsorption and stabilization of target analytes and prevent excessive separation and dispersion by creating clear detection zones. Probe–metal complexes are effectively detected by the naked eye and can be measured using inexpensive optical patterns.[90] Therefore, in this part of the study, the efficiency of paper microfluidics in the diagnosis of As(III) has been evaluated.

**3.4.1. Optimization of paper type for μPAD fabrication.** In the production of microfluidic paper chips, hydrophilic capillary channels are created on paper using hydrophobic materials, in which no chemical reaction takes place between cellulose and hydrophobic materials.[91] Different types of paper can be applied depending on the sensor application and how it is made. Because 30% to 90% of paper is porous and their shape is not the same in different types of paper, the structure of the pores can help in the use of papers in diverse fields. Therefore, the choice of paper type is of particular importance and several factors such as non-decomposition and deformation after immersion in the liquid phase, heat loss and sufficient tolerance must be considered in this selection.[92] In addition, microfluidic paper chips highly require water-absorbent paper. Therefore, filter paper can be considered the best matrix in the construction of microfluidic paper chips due to its large pores and high absorption ability.[93,94] In this work, filter paper and glass fiber paper were used to make microfluidic chips. These chips were employed to detect As(III) using sensing probes.

Zones 1 to 8 are associated with AgNPrs, Cys-capped AgNPrs, AgNPrs/As, Cys-capped Ag NPrs/As, Met-capped AgNPrs/As, Met-capped AgNPrs, AgNWs, and AgNWs/As, respectively. As shown in Fig. S25 (see ESI†), the microfluidic chip made of filter paper does not have good capillary and adsorption capability. However, glass fiber paper forms very good capillary channels and has a high fluid absorption capacity. Therefore, in this work, colorimetric identification was performed using microfluidic chips prepared from glass fiber paper.

**3.4.2. Colorimetric assay of As(III) using μPAD technology.** The experimental behavior of probes based on various types of Ag NPs was evaluated using the optical method and the results showed that the proposed probes are capable of detecting As(III) ions using μPADs. But the interesting thing is how such a diagnosis can be made on-site without the need for trained personnel. Therefore, there is a need to develop a practical, direct, rapid, and accurate method for the detection of As(III) by μPADs. Colorimetric methods can be visually used to identify semi-quantitative target analytes in real-time. Colorimetric assays were evaluated using paper-based microfluidic chips. Images of μPADs were taken under natural light, in which color changes of AgNPrs, AgNPrs with Cys cap, AgNPrs with a metal coating, and AgNWs probe were examined by non-capillary assay. As shown in Fig. S26 (see ESI†), colorimetric analyses on the surface of the μPADs confirm the results of the solution. However, the reaction of As(III) with hydroxyl and carboxyl groups on the surface of the sensing probes stabilized on the μPADs, is not as fast as the solution and does not change color immediately after analyte casting. Considering that no significant color change is seen in the presence of As(III) using the AgNWs probe, it can be concluded that this probe can't be used in the microfluidic colorimetric assay of this ion. The results revealed that the presented paper-based microchips can detect As(III) and they can be developed to provide on-site diagnostic kits.

**3.4.3. μPADs based colorimetric assay of As(III) in different media.** Due to the acceptable performance of microfluidics assay of As(III) using proposed probes, they were also employed for analytical analysis in standard and human urine specimens. For this purpose, first, the sensing probes were drop-cast in the sensing zone, then different concentrations of arsenic (zones 1 to 8 corresponding to the concentrations of 1, 0.8, 0.6, 0.3, 0.1, 0.05, 0.01, and 0.0005 ppm, respectively) were drop-cast on them. The recorded images were taken under natural light. As can be seen in Fig. S27 (see ESI†), the AgNPrs sensing probe shows significant color changes in zones 1 to 6, and it should be noted that the intensity of the color change is proportional to the analyte concentration. Also, no color change was observed in zones 7 and 8. Therefore, it can be said that the lowest concentration that is detected using μPAD modified by the AgNPrs probe is 0.05 ppm. But, in the other two sensing probes (Cys-capped AgNPrs and Met-capped AgNPrs), the discoloration was not proportional to the As(III) concentration. Therefore, they can't be used to test for arsenic quantitatively in μPCD. To further investigate of μPADs performance in real samples, the color changes of As(III) spiked in human urine samples were recorded. The μPADs were able to detect arsenic ions at high concentrations and did not show this capability at low concentrations. Therefore, it is necessary to conduct advanced research in this field through the concepts of mass and heat transfer to provide the ability to develop these tools. Concentration changes in color were not observed in all four detection probes (Fig. S28 (see ESI†)). Therefore, this method can only be used for qualitative evaluation of arsenic in urine. The results indicated that, among the presented sensing probes, AgNPrs have the best performance in the detection of As(III) by μPAD technology.

**3.4.4. Selectivity analyses of As(III) using μPADs modified by different Ag NPs.** μPADs were also employed to detect other ions using AgNPrs, Cys-capped AgNPrs, and Met-capped AgNPrs probes to investigate the specificity of the proposed tools. To do this, the probes were drop-cast on the sensing zone and different types of ions were immediately immobilized on them. The images were taken in natural light and after 3 minutes. As shown in Fig. 3, μPADs made from AgNPrs probes are unable to detect W(IV), Co(II), and Ni(II) (no color change in their presence). The color change in the presence of other ions is similar to As(III). Therefore, these μPADs can detect all ions with a different color. In the case of Cys-capped AgNPrs probes, the discoloration of Ti(II) and Fe(III) is different from that of arsenic, although Si(II), Co(II), Cs(II), and Ni(II) ions are not detectable with this probe. Other ions have the same color change as As(III), so this probe also detects other ions with different color changes in addition to As(III) and does not differentiate between them. The Met-capped AgNPrs probe, in addition to arsenic, detects other ions, including W(IV) and Bi(III), by similar color changes. While it detects Hg(II), Ti(II), Fe(III), Pt (II), V(III), and Zr(IV) with a different color change than arsenic, it can't detect other ions. The selectivity of the proposed probes was evaluated to specific recognition of As(III) in the presence of other ions. In the case of AgNPrs probes, Hg(II), Pt(II), Sr(II), V(III), Te(II), Si(II), and Ni(II) ions do not interfere with As(III) detection. In other words, the resulting color change is similar to As(III) itself. While other ions interfere with the detection of As(III) and cause different color changes. In the case of the Cys-capped AgNPrs probe, some ions like Hg(II), Zr(IV), Fe(III), V(III), Bi(III), Al(III), Ca(II), and Na(I) do not interfere on the performance of designed μPADs. Finally using the Met-capped AgNPrs probe, only ions Si(II) and Cs(II) interfere with the colorimetric method developed for the detection of As(III) using μPADs (Fig. 4).

**3.4.5. Investigation of nanoparticle-modified μPADs for long-term detection of As(III).** To investigate the possibility of developing μPADs to produce on-site diagnostic kits, the stability of the probes (AgNPrs, Cys-capped AgNPrs, and Met-capped AgNPrs) on the surface of the μPADs was evaluated. For this purpose, the μPADs were functionalized by drop-casting of optical sensing probes toward the colorimetric analysis of the target ion. As shown in Fig. 5, after drying at room temperature, the candidate Ag NPs aggregate, and their color turns purple. The drying and aggregation process takes about 10 minutes. The interaction of arsenic with the modified μPADs was then evaluated for 8 consecutive days. After drop-casting of As(III) in the sensing zone, it takes about 5 minutes to react between it and the dried NPs to change the color of the NPs to

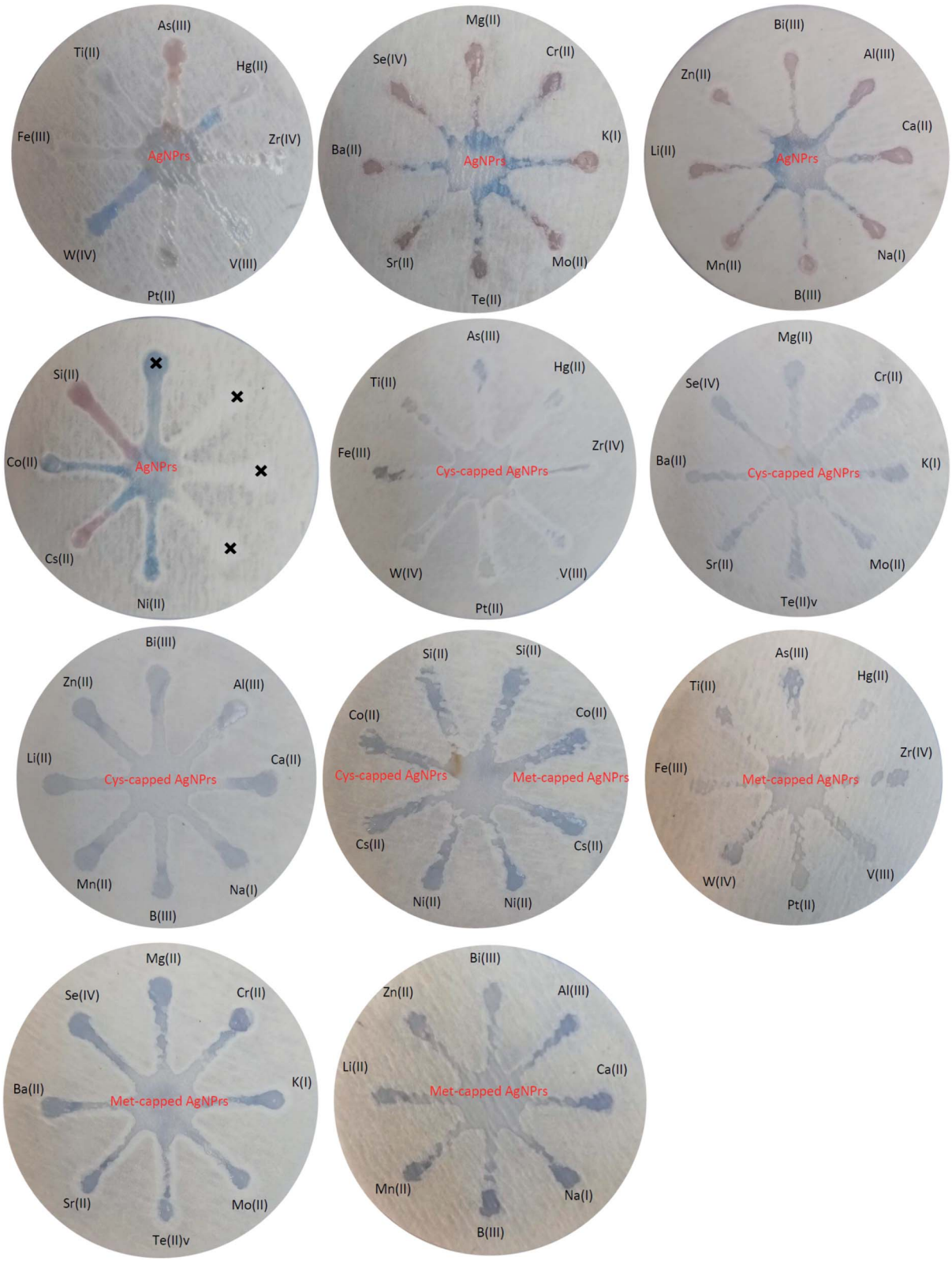


Fig. 3 Specificity analysis of chemosensing performance of optical probes for individual identification of some metal ions using μPADs.

colorless. According to the results, the introduced μPADs were able to detect arsenic within 8 days. This could be the beginning of the development of nanoparticle-modified μPADs for rapid and accurate identification of As(III). Optical interaction and optical properties between NPs and paper substrates are affected by the aggregation of NPs in cellulose fibers of the paper, the refractive index of paper, and the NPs spatial location. The penetration and aggregation of NPs in the porous

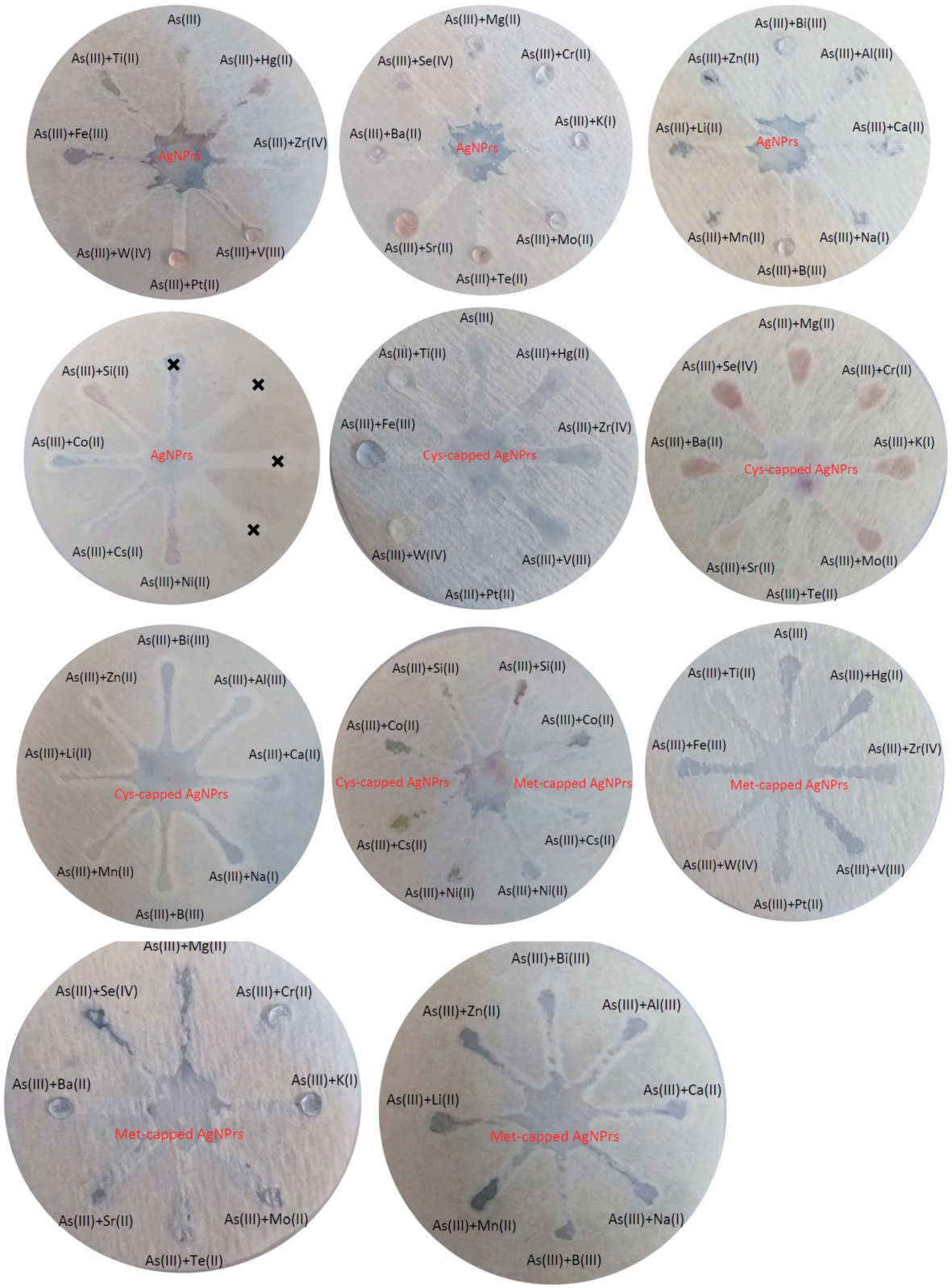


Fig. 4 Selectivity analysis of sensing probes for identification of As(III) in the presence of other metal ions using μPADs.

structure of the paper can cause different light interactions compared to a non-porous flat substrate. In fact, during the drying and aggregation process, the overall state of the NPs is maintained, which is very important in controlling their optical properties. However, the reproducibility of the aggregation and adsorption mode of NPs is limited by the random fibrous structure of the paper substrates.[95] Therefore, to produce on-site diagnostic kits, there is a need for more in-depth studies on the

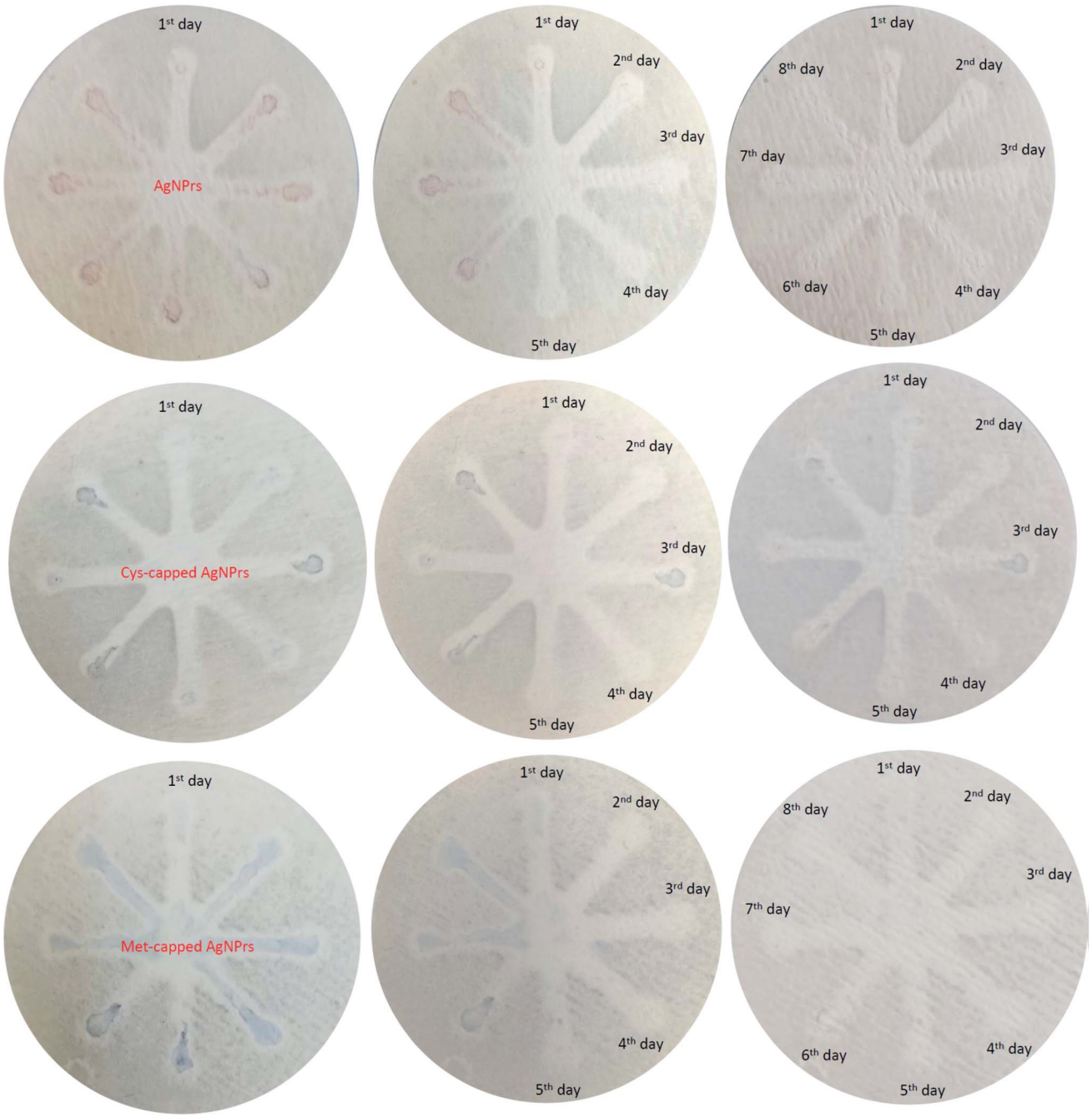


Fig. 5 Stability analysis of sensing probes immobilized in the surface of μPAD in different time of storages (1–8 days).

state of nanoparticle aggregation in paper layers, paper thickness, and an understanding of the optical properties of nanoparticle-modified paper.

## 4. Conclusion

In summary, this study presents a novel As(III) detection method based on changing the morphology of Ag NPrs. The Ag NPrs changed to a spherical shape as a result of the reduction–oxidation reaction between silver nitrate and As(III), and consequently, the deformation resulted in a rapid color change. Based on this phenomenon, a detection strategy with the naked eye of As(III) was developed. By measuring the UV-Vis absorption wavelength in developed systems, a fast visual method with As(III) analysis capability in the range of 0.0005 to 1 ppm with an LLOQ of 0.0005 ppm was presented. In addition to the quantitative analysis, we also qualitatively evaluated the capabilities of the presented paper-based microfluidic in the detection of As(III). We also assessed the potential of μPADs to build on-site diagnostic kits. The results revealed that nanoparticle-modified μPADs have long-term stability and can be utilized for long-term As(III) monitoring. Examination of the interferers also showed

that some ions interfere with the detection of As(III). Therefore, in future studies, it is necessary to control or eliminate all other interfering agents. In conclusion, an innovative, simple, inexpensive, and sensitive method was proposed for the monitoring of As(III) in real samples.

## Conflicts of interest

There are no conflicts to declare.

## Acknowledgements

We gratefully acknowledge Tabriz University of Medical Sciences for instrumental supporting of this research.

## References

1 B. Chen, Q. Liu, A. Popowich, S. Shen, X. Yan, Q. Zhang, X.-F. Li, M. Weinfeld, W. R. Cullen and X. C. Le, *Metallomics*, 2015, **7**, 39–55.
2 P. Nath, N. Priyadarshni and N. Chanda, *ACS Appl. Nano Mater.*, 2017, **1**, 73–81.
3 J. Li, B. Zheng, Z. Zheng, Y. Li and J. Wang, *Sensors and Actuators Reports*, 2020, **2**, 100013.
4 B. Zheng, J. Li, Z. Zheng, C. Zhang, C. Huang, J. Hong, Y. Li and J. Wang, *Opt. Laser Technol.*, 2021, **133**, 106522.
5 S. H. Koli, B. V. Mohite, R. K. Suryawanshi, H. P. Borase and S. V. Patil, *Bioprocess Biosyst. Eng.*, 2018, **41**, 715–727.
6 L. Gong, B. Du, L. Pan, Q. Liu, K. Yang, W. Wang, H. Zhao, L. Wu and Y. He, *Microchim. Acta*, 2017, **184**, 1185–1190.
7 P. K. Sarkar, A. Halder, N. Polley and S. K. Pal, *Water, Air, Soil Pollut.*, 2017, **228**, 1–11.
8 N. Yogarajah and S. S. Tsai, *Environ. Sci.: Water Res. Technol.*, 2015, **1**, 426–447.
9 Z.-G. Liu and X.-J. Huang, *TrAC, Trends Anal. Chem.*, 2014, **60**, 25–35.
10 A. Rahman, S. Kumar, A. Bafana, S. A. Dahoumane and C. Jeffryes, *Molecules*, 2019, **24**, 98.
11 G. Vyas, S. Bhatt and P. Paul, *ACS Omega*, 2019, **4**, 3860–3870.
12 H. Guan, X. Liu, W. Wang and J. Liang, *Spectrochim. Acta, Part A*, 2014, **121**, 527–532.
13 P. C. Mane, M. D. Shinde, S. Varma, B. P. Chaudhari, A. Fatehmulla, M. Shahabuddin, D. P. Amalnerkar, A. M. Aldhafiri and R. D. Chaudhari, *Sci. Rep.*, 2020, **10**, 1–14.
14 H. Revanasiddappa, B. Dayananda and T. Kumar, *Environ. Chem. Lett.*, 2007, **5**, 151–155.
15 G. P. Pincetti-Zúniga, L. A. Richards, Y. M. Tun, H. P. Aung, A. K. Swar, U. P. Reh, T. Khaing, M. M. Hlaing, T. A. Myint and M. L. Nwe, *Appl. Geochem.*, 2020, **115**, 104535.
16 H. Li, Z. Cui and C. Han, *Sens. Actuators, B*, 2009, **143**, 87–92.
17 T. H. A. Nguyen, V.-C. Nguyen, T. N. H. Phan, Y. Vasseghian, M. A. Trubitsyn, A.-T. Nguyen, T. P. Chau and V.-D. Doan, *Chemosphere*, 2022, **287**, 132271.
18 P. Prema, V. Veeramanikandan, K. Rameshkumar, M. K. Gatasheh, A. A. Hatamleh, R. Balasubramani and P. Balaji, *Environ. Res.*, 2022, **204**, 111915.
19 S. Bhatt, G. Vyas and P. Paul, *ACS Omega*, 2022, **7**(1), 1318–1328.
20 J. Ji, H. Wu, D. Wang, D. Liu, X. Chen and S. Feng, *Anal. Methods*, 2022, **14**(6), 643–651.
21 Y. Yu, S. S. Naik, Y. Oh, J. Theerthagiri, S. J. Lee and M. Y. Choi, *J. Hazard. Mater.*, 2021, **420**, 126585.
22 T. T.-T. Ho, C.-H. Dang, T. K.-C. Huynh, T. K.-D. Hoang and T.-D. Nguyen, *Carbohydr. Polym.*, 2021, **251**, 116998.
23 F. Li, T. He, S. Wu, Z. Peng, P. Qiu and X. Tang, *Microchem. J.*, 2021, **164**, 105987.
24 E. Priyadarshini and N. Pradhan, *Sens. Actuators, B*, 2017, **238**, 888–902.
25 C. Wang and C. Yu, *Rev. Anal. Chem.*, 2013, **32**, 1–14.
26 F. Li, J. Wang, Y. Lai, C. Wu, S. Sun, Y. He and H. Ma, *Biosens. Bioelectron.*, 2013, **39**, 82–87.
27 M. Sabela, S. Balme, M. Bechelany, J. M. Janot and K. Bisetty, *Adv. Eng. Mater.*, 2017, **19**, 1700270.
28 C. Liu, Q. Pang, T. Wu, W. Qi, W. Fu and Y. Wang, *J. Anal. Test.*, 2021, 1–7.
29 M. A. Mahmud, E. J. Blondeel, M. Kaddoura and B. D. MacDonald, *Analyst*, 2016, **141**, 6449–6454.
30 M. M. Gong, P. Zhang, B. D. MacDonald and D. Sinton, *Anal. Chem.*, 2014, **86**, 8090–8097.
31 M. A. Chowdury, N. Walji, M. Mahmud and B. D. MacDonald, *Micromachines*, 2017, **8**, 71.
32 A. Tribhuwan Singh, D. Lantigua, A. Meka, S. Taing, M. Pandher and G. Camci-Unal, *Sensors*, 2018, **18**, 2838.
33 S. Nishat, A. T. Jafry, A. W. Martinez and F. R. Awan, *Sens. Actuators, B*, 2021, 129681.
34 P. Abdollahiyan, M. Hasanzadeh, F. Seidi and P. Pashazadeh-Panahi, *J. Environ. Chem. Eng.*, 2021, **9**, 106197.
35 Y. Sun, B. Mayers, T. Herricks and Y. Xia, *Nano Lett.*, 2003, **3**, 955–960.
36 A. Saadati, F. Farshchi, M. Hasanzadeh and F. Seidi, *Anal. Methods*, 2021, **13**, 3909–3921.
37 F. Farshchi, A. Saadati, M. Hasanzadeh and F. Seidi, *RSC Adv.*, 2021, **11**, 27298–27308.
38 Y. Wang, C. Wang, L. Wang, L. Wang and F.-S. Xiao, *Acc. Chem. Res.*, 2021, **54**, 2579–2590.
39 C.-C. Wang, H.-T. Yau and C.-C. Wang, *Math. Probl. Eng.*, 2013, **2013**, 143–149.
40 N. L. Rosi and C. A. Mirkin, *Chem. Rev.*, 2005, **105**, 1547–1562.
41 D. V. Talapin, J.-S. Lee, M. V. Kovalenko and E. V. Shevchenko, *Chem. Rev.*, 2010, **110**, 389–458.
42 Y.-L. Hung, T.-M. Hsiung, Y.-Y. Chen, Y.-F. Huang and C.-C. Huang, *J. Phys. Chem. C*, 2010, **114**, 16329–16334.
43 A. K. Jain, V. K. Gupta, B. B. Sahoo and L. P. Singh, *Anal. Proc.*, 1995, **32**, 99–101.
44 Y. Li, P. Wang, X. Wang, M. Cao, Y. Xia, C. Cao, M. Liu and C. Zhu, *Microchim. Acta*, 2010, **169**, 65–71.
45 A. Gutiérrez-Blanco, C. Dobbe, A. Hepp, C. G. Daniliuc, M. Poyatos, F. E. Hahn and E. Peris, *Eur. J. Inorg. Chem.*, 2021, **2021**, 2442–2451.

46 L. Xing, Q. Zhao, X. Zheng, M. Hui, Y. Peng, X. Zhu, L. Hu, W. Yao and Z. Yan, *ACS Appl. Nano Mater.*, 2021, **4**, 3639–3646.
47 V. K. Gupta, A. K. Singh and L. K. Kumawat, *Sens. Actuators, B*, 2014, **195**, 98–108.
48 K. Siriwardana, A. Wang, M. Gadogbe, W. E. Collier, N. C. Fitzkee and D. Zhang, *J. Phys. Chem. C*, 2015, **119**, 2910–2916.
49 G. S. Métraux and C. A. Mirkin, *Adv. Mater.*, 2005, **17**, 412–415.
50 J. E. Millstone, S. J. Hurst, G. S. Métraux, J. I. Cutler and C. A. Mirkin, *Small*, 2009, **5**, 646–664.
51 P. Abdollahiyan, M. Hasanzadeh, P. Pashazadeh-Panahi and F. Seidi, *J. Mol. Liq.*, 2021, **338**, 117020.
52 G. Wang, W. Wang, J. Wu, H. Liu, S. Jiao and B. Fang, *Microchim. Acta*, 2009, **164**, 149–155.
53 N. Kumar and L. S. B. Upadhyay, *Appl. Surf. Sci.*, 2016, **385**, 225–233.
54 F. Bamdad, F. Khorram, M. Samet, K. Bamdad, M. R. Sangi and F. Allahbakhshi, *Spectrochim. Acta, Part A*, 2016, **161**, 52–57.
55 J. Li, L. Chen, T. Lou and Y. Wang, *ACS Appl. Mater. Interfaces*, 2011, **3**, 3936–3941.
56 P. Mulpur, A. Kurdekar, R. Podila, A. M. Rao and V. Kamisetti, *Nanotechnol. Rev.*, 2015, **4**, 393–400.
57 Y. Sun, X. Wang and H. Zhang, *Biosensors*, 2022, **12**, 382.
58 P. Prosposito, L. Burratti and I. Venditti, *Chemosensors*, 2020, **8**, 26.
59 T. Poonia, N. Singh and M. Garg, *Int. J. Environ. Sci. Technol.*, 2021, 1–12.
60 D. Vilela, M. C. González and A. Escarpa, *Anal. Chim. Acta*, 2012, **751**, 24–43.
61 C. V. Restrepo and C. C. Villa, *Environ. Nanotechnol., Monit. Manage.*, 2021, **15**, 100428.
62 K. M. Mayer and J. H. Hafner, *Chem. Rev.*, 2011, **111**, 3828–3857.
63 S. Szunerits and R. Boukherroub, *Chem. Commun.*, 2012, **48**, 8999–9010.
64 K. Shiva Prasad, G. Shruthi and C. Shivamallu, *Sensors*, 2018, **18**, 2698.
65 K. A. Willets and R. P. Van Duyne, *Annu. Rev. Phys. Chem.*, 2007, **58**, 267–297.
66 V. N. Mehta, A. K. Mungara and S. K. Kailasa, *Anal. Methods*, 2013, **5**, 1818–1822.
67 S. Diamai and D. P. Negi, *Spectrochim. Acta, Part A*, 2019, **215**, 203–208.
68 B. Malile and J. I. Chen, *J. Am. Chem. Soc.*, 2013, **135**, 16042–16045.
69 S.-H. Wen, R.-P. Liang, L. Zhang and J.-D. Qiu, *ACS Sustainable Chem. Eng.*, 2018, **6**, 6223–6232.
70 W. Siangproh, O. Chailapakul and K. Songsrirote, *Talanta*, 2016, **153**, 197–202.
71 F. Divsar, K. Habibzadeh, S. Shariati and M. Shahriarinour, *Anal. Methods*, 2015, **7**, 4568–4576.
72 B. S. Boruah, N. K. Daimari and R. Biswas, *Results Phys.*, 2019, **12**, 2061–2065.
73 S. Kapaj, H. Peterson, K. Liber and P. Bhattacharya, *J. Environ. Sci. Health, Part A: Toxic/Hazard. Subst. Environ. Eng.*, 2006, **41**, 2399–2428.
74 Q. Y. Chen and M. Costa, *Annu. Rev. Pharmacol. Toxicol.*, 2021, **61**, 47–63.
75 S. N. Kales, K. L. Huyck and R. H. Goldman, *J. Anal. Toxicol.*, 2006, **30**, 80–85.
76 K. Yamanaka, H. Hayashi, M. Tachikawa, K. Kato, A. Hasegawa, N. Oku and S. Okada, *Mutat. Res., Genet. Toxicol. Environ. Mutagen.*, 1997, **394**, 95–101.
77 E. Shaji, M. Santosh, K. Sarath, P. Prakash, V. Deepchand and B. Divya, *Geosci. Front.*, 2021, **12**, 101079.
78 J. T. Hindmarsh, *Clin. Biochem.*, 2002, **35**, 1–11.
79 R. R. Lauwerys and P. Hoet, *Industrial chemical exposure: guidelines for biological monitoring*, CRC Press, 2001.
80 M. Ozturk, M. Metin, V. Altay, R. A. Bhat, M. Ejaz, A. Gul, B. T. Unal, M. Hasanuzzaman, L. Nibir and K. Nahar, *Biol. Trace Elem. Res.*, 2021, 1–14.
81 H. Ismail, M. N. Ahmad and E. Normaya, *Sci. Rep.*, 2021, **11**, 1–12.
82 P. W. Cheah, M. P. Heng, H. M. Saad, K. S. Sim and K. W. Tan, *Opt. Mater.*, 2021, **114**, 110990.
83 A. Sanfeld and A. Steinchen, *Surf. Sci.*, 2000, **463**, 157–173.
84 N. Yekeen, T. X. Kun, A. Al-Yaseri, F. Sagala and A. K. Idris, *J. Mol. Liq.*, 2021, **338**, 116658.
85 Y. Cao, Z. Chen, X. Li, Z. Li, G. Lin, T. Liu and Y. Wu, *Anal. Chim. Acta*, 2022, 339998.
86 E. A. Syukkalova, A. V. Sadetskaya, N. D. Demidova, N. P. Bobrysheva, M. G. Osmolowsky, M. A. Voznesenskiy and O. M. Osmolovskaya, *Ceram. Int.*, 2021, **47**, 2809–2821.
87 H. Doi, T. Watanabe, N. Nishizawa, T. Saito, H. Nagata, Y. Kameda, N. Maki, K. Ikeda and T. Fukuzawa, *Mol. Ecol. Resour.*, 2021, **21**, 2364–2368.
88 I. Jang, D. B. Carrão, R. F. Menger, A. R. Moraes de Oliveira and C. S. Henry, *ACS Sens.*, 2020, **5**, 2230–2238.
89 V. Abergel, K. Jacquot, L. De Luca and P. Veron, *Disegnarecon*, 2021, **14**, 1310–1314.
90 H. Manisha, P. P. Shwetha and K. Prasad, in *Environmental, Chemical and Medical Sensors*, Springer, 2018, pp. 315–341.
91 X. Qin, J. Liu, Z. Zhang, J. Li, L. Yuan, Z. Zhang and L. Chen, *TrAC, Trends Anal. Chem.*, 2021, **143**, 116371.
92 W. Zhou, M. Dou, S. S. Timilsina, F. Xu and X. Li, *Lab Chip*, 2021, **21**, 2658–2683.
93 L. J. Loh, G. C. Bandara, G. L. Weber and V. T. Remcho, *Analyst*, 2015, **140**, 5501–5507.
94 K. M. Schilling, A. L. Lepore, J. A. Kurian and A. W. Martinez, *Anal. Chem.*, 2012, **84**, 1579–1585.
95 Y. H. Ngo, D. Li, G. P. Simon and G. Garnier, *Adv. Colloid Interface Sci.*, 2011, **163**, 23–38.